Optics Letters

Tunable SNAP microresonators via internal ohmic heating

Dashiell L. P. Vitullo,[1,*] Sajid Zaki,[1] Gabriella Gardosi,[1] Brian J. Mangan,[2] Robert S. Windeler,[2] Michael Brodsky,[3] and Misha Sumetsky[1]

[1]Aston Institute of Photonic Technologies, Aston University, Birmigham B4 7ET, UK
[2]OFS Laboratories, Somerset, New Jersey 08873, USA
[3]U.S. Army Research Laboratory, Adelphi, Maryland 20783-1197, USA
*Corresponding author: vitullod+journal@gmail.com

Received 16 May 2018; revised 19 June 2018; accepted 1 July 2018; posted 3 July 2018 (Doc. ID 331025); published 31 August 2018

We demonstrate a thermally tunable surface nanoscale axial photonics (SNAP) platform. Stable tuning is achieved by heating a SNAP structure fabricated on the surface of a silica capillary with a metal wire positioned inside. Heating a SNAP microresonator with a uniform wire introduces uniform variation of its effective radius which results in constant shift of its resonance wavelengths. Heating with a nonuniform wire allows local nanoscale variation of the capillary effective radius, which enables differential tuning of the spectrum of SNAP structures, as well as the creation of temporary SNAP microresonators that exist only when current is applied. As an example, we fabricate two bottle microresonators coupled to each other and demonstrate differential tuning of their resonance wavelengths into and out of degeneracy with precision better than 0.2 pm. The developed approach is beneficial for ultra-precise fabrication of tunable ultralow loss parity-time symmetric, optomechanical, and cavity quantum electrodynamics (QED) devices.

OCIS codes: (060.2340) Fiber optics components; (140.3945) Microcavities; (230.3990) Micro-optical devices.

https://doi.org/10.1364/OL.43.004316

Optical high Q-factor microresonators are basic elements for a diverse range of photonic devices with applications including optical telecommunications through delay lines, switches, and buffers [1–3]; frequency comb generation [4,5]; optomechanics [6]; and quantum information [7–11]. The capability to tune microresonators is necessary for many of these applications. It is often required that ultrahigh Q-factor microresonators [e.g., those used in parity-time symmetry [12,13] and quantum electrodynamics (QED) [11] investigations] be tunable with ultrahigh precision comparable to their narrow linewidths. While the technology for fabrication of tunable microresonator devices is well developed in silicon photonics [14] and has been demonstrated for individual toroidal and spherical microresonators (see e.g., [12,15,16]), the achieved precision of fabrication and tunability is still not sufficient for several applications [2]. On the other hand, the surface nanoscale axial photonics (SNAP) platform, which utilizes whispering gallery mode microresonators fabricated on the surfaces of optical fibers, boasts microresonators with ultralow loss and record fabrication precision better than 20 pm in effective radius variation (ERV) [17,18]. The unique capabilities of this technology suggest it can enable new breakthrough applications, provided that SNAP structures are made tunable.

In this Letter, we present a thermally tunable SNAP platform which is realized for SNAP structures fabricated on the surface of a silica capillary heated with a metal wire positioned inside (Fig. 1). Specifically, we demonstrate global tuning of entire SNAP microresonators, creation of temporary microresonators that exist only when heat is applied, and local differential tuning that controls the separation between the resonance wavelengths of adjacent microresonators. We demonstrate differential tuning with precision better than 0.2 pm in wavelength variation, which is a 6× improvement over the 1.3 pm precision demonstrated with post-processing [17]. The creation of temporary SNAP microresonators introduced by local heating with a CO_2 laser has been previously demonstrated and indicates a thermal microresonator response time of order 10 μs [19]. However, ohmic heating with an internal wire allows designs that are substantially more compact, flexible, and inexpensive.

The effective radius is a combination of the refractive index and the physical radius, and whispering gallery modes guided along a surface can be exquisitely sensitive to its ERV [18]. A SNAP bottle microresonator is made by inducing a small bump (nanometer scale height for a fiber with a 10 μm scale diameter) in the effective radius profile, which confines whispering gallery modes in the longitudinal direction. The modes of these microresonators are solutions to the 1D Schrödinger equation, where the one spatial dimension is along the longitudinal fiber axis (z). The potential, which we aim to control in this Letter, is proportional to the change in the ERV. The resonance spectrum of the modes can be monitored by placing a tapered fiber in contact with the SNAP microresonator and monitoring

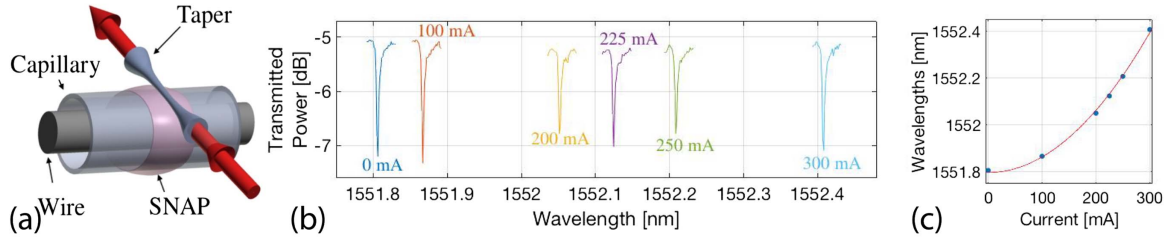

Fig. 1. (a) Illustration of stable tuning using a uniform wire inside a capillary with a laser-induced SNAP resonator, monitored with a tapered fiber. Objects are not to scale. (b) Resonance wavelength tuning of a single microresonator mode over $\Delta\lambda = 0.6$ nm. (c) Resonance wavelength versus current I. The points are measured values, and the red line shows the best parabolic fit $\lambda(I) = 1551.8 + 6.6432 \times 10^{-6} I^2$.

the power transmission spectrum through the taper with an optical spectrum analyzer. The transmitted power has narrow dips at modal resonance wavelengths. A spatial map of resonant modes, referred to as a spectrogram, is made by serially measuring the transmission spectrum through the taper at a grid of positions on the microresonator, following the procedure described in Ref. [18]. The axial mode series shown, for example, in Figs. 2(b) and 2(c), has close wavelength spacing and indicates the shape of the microresonator profile, with the fundamental axial resonance at the longest wavelength and the higher-order axial resonances at sequentially shorter wavelengths. The mode structure is bounded from above by a cutoff wavelength, where the longitudinal component of the modal wavevector goes to zero.

Heating a SNAP microresonator modifies both the refractive index n and the radius r of the fiber, but the refractive index change dominates near room temperature, as dn/dT is roughly 17× greater than dr/dT [20]. Thus, thermal expansion of the radius can be neglected in an approximate relationship between temperature change ΔT and resonant wavelength change $\Delta\lambda$:

$$\Delta T = n_0 \left(\frac{\mathrm{d}n}{\mathrm{d}T}\right)^{-1} \frac{\Delta\lambda}{\lambda_0}, \tag{1}$$

where λ_0 is the initial resonance wavelength, and we use $n_0 = 1.44$ as the initial refractive index of fused silica and $\frac{dn}{dT} = 1.2 \times 10^{-5}/\mathrm{K}$. For a uniformly heated microresonator, the resonance wavelength shift of each mode is the same $\Delta\lambda$, and any mode can be chosen to calculate ΔT.

Our first attempts at tuning a SNAP microresonator involved local heating by placing a tungsten wire in contact with the fiber surface near the microresonator, but not in contact with it so as to avoid inducing loss. This method thermally shifted the resonance wavelengths, but the tuning was unstable and the central resonance wavelength fluctuated by much more than the resonance linewidth on a 1 s timescale. The observed fluctuations stemmed from air currents induced by the heated wire. To minimize the effect of air currents, we changed our design to use a hollow capillary fiber with a heating wire positioned inside it, as shown in Fig. 1(a). The capillary fiber, fabricated at OFS Laboratories, has a 188 μm outer diameter and 10 μm thick walls. With this thickness, the whispering gallery modes of the SNAP microresonator have negligible field amplitude at the inner capillary surface and are unaffected by introduction of material into the capillary interior. We install a 50 μm diameter tungsten heating wire connected to a DC power supply in constant current mode. This design demonstrates stable tuning.

The simplest version of SNAP microresonator tuning that we experimentally demonstrate utilizes a uniform wire to tune a laser-induced microresonator, as illustrated in Fig. 1. Uniform temperature tuning does not change the shape of capillary ERV,

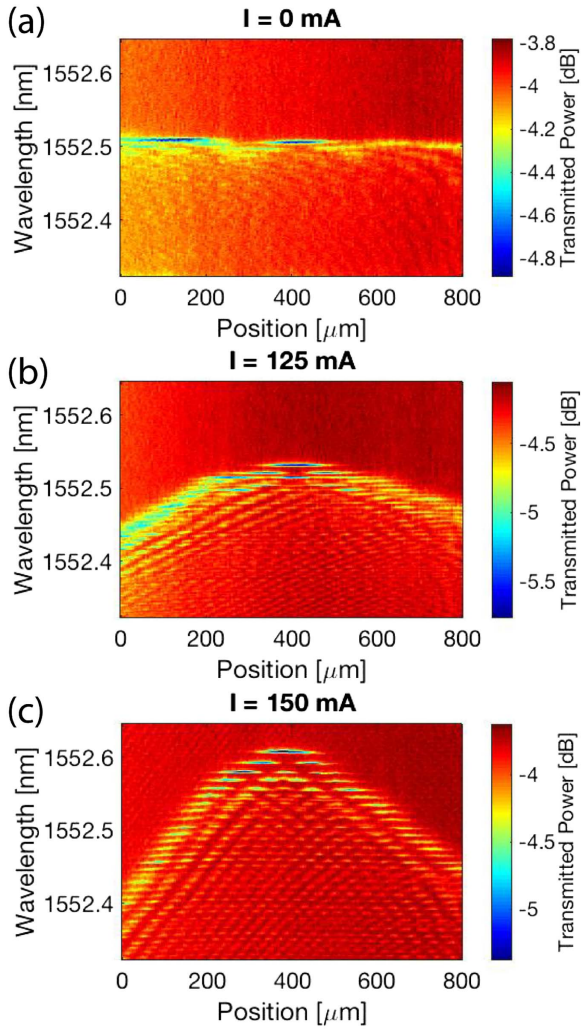

Fig. 2. Temporary SNAP spectrograms with identical wavelength and distance ranges sampled on a uniform position grid with 5 μm spacing. We observe repeatable microresonator induction and annihilation, and present spectrograms of the microresonator at (a) $I = 0$ mA, (b) $I = 125$ mA, and (c) $I = 150$ mA. Subfigures (b) and (c) show the same axial mode series, which is below the wavelength window of (a).

so the resonance wavelengths of microresonator modes are equally shifted in wavelength space and, therefore, maintain their relative spacings. As shown in Fig. 1(b), the shift in resonance wavelength from $I = 0$ mA to $I = 300$ mA is $\Delta\lambda = 0.6$ nm, which corresponds through Eq. (1) to a temperature change of $\Delta T = 46.6$°C. The resonator structure and line shapes do not change with tuning [see Fig. 1(b)]. The resonance wavelengths are stable on second timescales, though environmental temperature drifts can still cause few-minute timescale fluctuations, which could be addressed with a feedback loop connected to the current supply to stabilize the resonance wavelength.

Heating with a nonuniform wire allows localized deformation of the ERV. The resistance of a wire $R(z) \propto 1/A(z)$, where $A(z)$ is the local cross-sectional area. The change in the ERV from ohmic heating is proportional to the heating profile $\Delta T(z)$, which can be determined from the local power dissipated in the wire:

$$P(z) = I^2 R(z). \tag{2}$$

Chemical etching enables targeted reduction of the wire diameter, and heating is maximal at the wire waist, where the diameter is smallest [see Eq. (2)]. In our experiment, we use tungsten wire with a 50 μm initial diameter etched over a small region in hydrogen peroxide (H_2O_2) [21]. Care must be taken when preparing the wire to avoid inducing kinks, which can break the capillary upon insertion. Etching the wire in a bath of H_2O_2 at 50°C reaches the target diameter of $15 < d < 20$ μm in a few hours. Surface tension and adhesive forces limit the smallest etched region length practically achievable with this method to ∼1 mm.

Heating a uniform capillary with an etched wire can create temporary SNAP microresonators that appear when heating is applied and disappear when heating stops. We demonstrate this experimentally with an etched wire with a 15 μm diameter waist and ∼3 mm extent in Fig. 2. The number of axial modes and the wavelength separation between them increases with the current. The height of the microresonator in wavelength space can exceed the separation between adjacent modes with different azimuthal or radial quantum numbers.

Despite nonuniform tuning, Eq. (1) can be used to approximate the maximal temperature shift of a temporary SNAP microresonator if $\Delta\lambda$ is interpreted not as the shift of the resonance wavelength of any arbitrary mode, but as the shift of the maximal cutoff wavelength, which is well approximated by the wavelength of the fundamental axial resonance. The maximal temperature change at $I = 150$ mA occurs with $\Delta\lambda = 1.84$ nm, so Eq. (1) gives $\Delta T = 143$°C. The induction of permanent SNAP structures requires heating into fused silica's annealing temperature regime, and the temperatures achieved here are far below that regime, so the changes induced by heating are reversible.

Nonuniform wires enable differential tuning of photonic circuit elements. We demonstrate this with a microresonator structure consisting of two laser-induced coupled microresonators, diagrammed in Fig. 3(a). The lowest-order axial modes are made to have distinct initial resonance wavelengths, with the left resonance (L) 6 pm below the right resonance [R, see Fig. 3(b)]. The etched wire used here has a waist diameter of 17.7 μm over a 2 mm etched region. Positioning an etched wire with the waist closer to the feature with smaller resonance

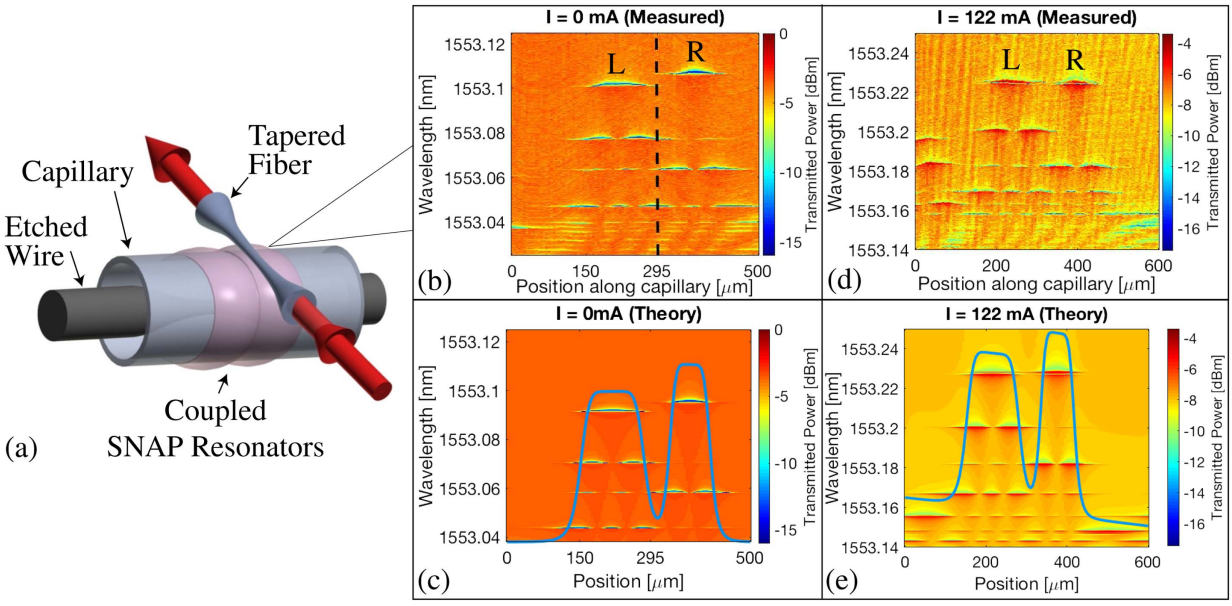

Fig. 3. (a) Illustration of differentially tunable coupled SNAP microresonators. An etched wire is placed in a capillary with two coupled SNAP microresonators on the surface. The waist of the etched region is positioned to heat the left resonator more than the right resonator. Objects are not to scale. (b) Spectrogram of the coupled microresonators with no applied current. The left and right fundamental axial resonances are labeled L and R, respectively. Positioning the probe on the dashed line monitors the resonance wavelengths of all modes simultaneously. The spectral resolution is 141 fm, and the grid spacing is 5 μm. This mode structure is theoretically reconstructed in (c) with the ERV profile (in wavelength scale) overlaid in blue. (d) Measured spectrogram with heating current $I = 122$ mA. The grid spacing is 4 μm, and the spectral resolution is 8 fm (1 MHz). Heating causes additional unwanted coupling of a neighboring feature into the original mode structure, but this does not affect the splitting of L and R. (e) Theoretical reconstruction of (d). The effective radius differs from (c) by a linear heating profile only. The profile indicates that the temperature change from Eq. (1) is $\Delta T_L = 10.64$°C at peak L, and $\Delta T_R = 10.19$°C at R.

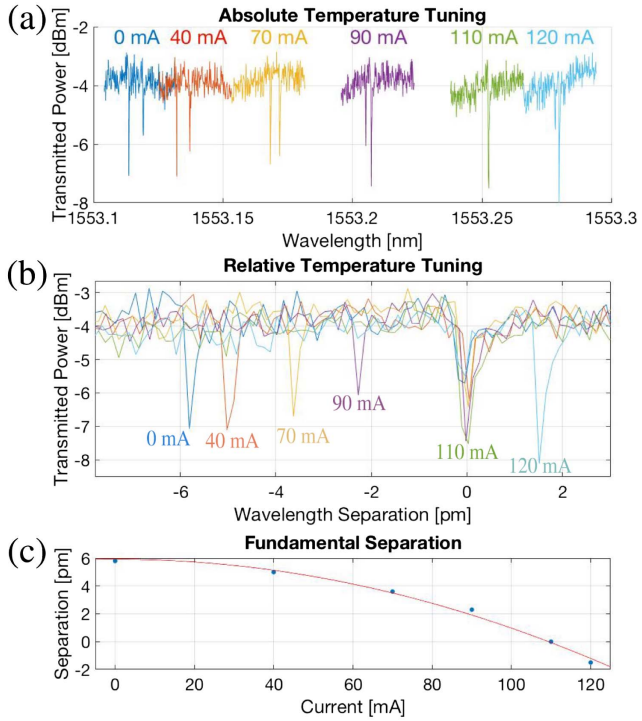

Fig. 4. Controlling the separation of fundamental resonance wavelengths $\lambda_R - \lambda_L$, with nonuniform heating. (a) Spectra showing resonant transmission dips for L and R at several current settings. All resonances are shifted to higher wavelengths as the capillary is heated, but L is shifted more than R as it is closer to the wire waist. (b) Shifts common to both L and R are subtracted by translating the wavelengths such that all the resonances of mode R overlap at zero separation, revealing the separation as a function of current. (c) Separation $\delta\lambda(I) = \lambda_R(I) - \lambda_L(I)$ versus current I. Tuning is parabolic as a function of current, since $\Delta T \propto P = I^2 R$. Thus, the red curve is the best parabolic fit $\delta\lambda(I) = 5.927 - 4.954 \times 10^{-4} I^2$ of the blue points, which represent measured values.

wavelength (L, in this case) sets $\frac{d\lambda_L}{dI} > \frac{d\lambda_R}{dI}$, which allows the wavelength separation to be reduced into and past degeneracy. This is shown in Fig. 3(d), where λ_L is tuned to be slightly larger than λ_R and the split modal resonances indicate avoided crossing behavior. The heating induces a neighboring SNAP feature near position 0 μm in Fig. 3(d), but this does not affect the behavior of our modes of interest, L and R, in the range of reported currents. Ambient temperature fluctuations over the course of this ~30-minute scan shift the resonance frequencies. Eigenfrequencies are single-valued, so we correct for these fluctuations in our analysis by shifting the measured wavelength arrays to enforce that modes have a single resonance frequency.

Evanescent coupling between L and R allows their resonance wavelengths to be simultaneously monitored by placing the probe taper at the position indicated by the dashed line in Fig. 3(b). Control of the separation between the resonance dips for L and R is demonstrated in Fig. 4. Temperature drift causes the minor variation between the unheated fundamental resonances in Figs. 3(b) and 4(a). Figure 4(b) highlights the effect of heating on the separation between L and R. Degeneracy of the L and R resonances is achieved at $I = 110$ mA, and the anti-crossing splitting (i.e., the smallest achievable separation) is visible in Fig. 3(d), but is too small to be resolved at degeneracy. The tuning precision achieved here is better than the linewidth, setting a limit of 0.2 pm.

In conclusion, we demonstrate techniques for stable tuning of high Q-factor SNAP microresonators fabricated on the surface of a fused silica capillary fiber. The shape of the wire in the capillary controls the heating profile, allowing uniform and targeted differential tuning. The demonstrated tuning precision is better than 0.2 pm (i.e., six times more accurate than that achieved by static post-processing [17]) and is here limited only by the Q-factor of the fabricated microresonator ~10^7 (0.15 pm resonance width) and the resolution of the optical spectrum analyzer. This paves the way for using SNAP technology in the investigation of parity-time symmetry [12,13], optomechanics [6], cavity QED [7,8], and quantum many-body phenomena [22].

Funding. Royal Society (Wolfson Research Merit Award WM130110); Horizon 2020 Framework Programme (H2020) (H2020-EU.1.3.3, 691011); Engineering and Physical Sciences Research Council (EPSRC) (EP/P006183/1); Army Research Laboratory (ARL) (W911NF-17-2-0048).

Acknowledgment. M. S. acknowledges the Royal Society Wolfson Research Merit Award.

REFERENCES

1. E. F. Burmeister, D. J. Blumenthal, and J. E. Bowers, Opt. Switch. Netw. **5**, 10 (2008).
2. W. Bogaerts, M. Fiers, and P. Dumon, IEEE J. Sel. Top. Quantum Electron. **20**, 1 (2014).
3. M. Sumetsky, Phys. Rev. Lett. **111**, 1 (2013).
4. T. J. Kippenberg, R. Holzwarth, and S. A. Diddams, Science **332**, 555 (2011).
5. V. Dvoyrin and M. Sumetsky, Opt. Lett. **41**, 5547 (2016).
6. G. Bahl, J. Zehnpfennig, M. Tomes, and T. Carmon, Nat. Commun. **2**, 403 (2011).
7. J. Volz, M. Scheucher, C. Junge, and A. Rauschenbeutel, Nat. Photonics **8**, 965 (2014).
8. T. G. Tiecke, J. D. Thompson, N. P. De Leon, L. R. Liu, V. Vuletić, and M. D. Lukin, Nature **508**, 241 (2014).
9. J. Notaros, J. Mower, M. Heuck, C. Lupo, N. C. Harris, G. R. Steinbrecher, D. Bunandar, T. Baehr-Jones, M. Hochberg, S. Lloyd, and D. Englund, Opt. Express **25**, 21275 (2017).
10. D. V. Strekalov, C. Marquardt, A. B. Matsko, H. G. L. Schwefel, and G. Leuchs, J. Opt. **18**, 123002 (2016).
11. A. Reiserer and G. Rempe, Rev. Mod. Phys. **87**, 1379 (2015).
12. B. Peng, S. K. Ozdemir, F. Lei, F. Monifi, M. Gianfreda, G. L. Long, S. Fan, F. Nori, C. M. Bender, and L. Yang, Nat. Phys. **10**, 394 (2014).
13. L. Feng, R. El-Ganainy, and L. Ge, Nat. Photonics **11**, 752 (2017).
14. F. Morichetti, C. Ferrari, A. Canciamilla, and A. Melloni, Laser Photonics Rev. **6**, 74 (2012).
15. K. N. Dinyari, R. J. Barbour, D. A. Golter, and H. Wang, Opt. Express **19**, 17966 (2011).
16. R. Madugani, Y. Yang, J. M. Ward, J. D. Riordan, S. Coppola, V. Vespini, S. Grilli, A. Finizio, P. Ferraro, and S. N. Chormaic, Opt. Lett. **37**, 4762 (2012).
17. N. A. Toropov and M. Sumetsky, Opt. Lett. **41**, 2278 (2016).
18. M. Sumetsky, Nanophotonics **2**, 393 (2013).
19. A. Dmitriev, N. Toropov, and M. Sumetsky, *IEEE Photonics Conference IPC* (2015).
20. M. J. Weber, *Handbook of Optical Materials*, Laser & Optical Science & Technology (Taylor & Francis, 2002).
21. K. R. Williams, K. Gupta, and M. Wasilik, J. Microelectromech. Syst. **12**, 761 (2003).
22. M. J. Hartmann, F. G. Brandão, and M. B. Plenio, Laser Photonics Rev. **2**, 527 (2008).